A finite element model to improve noise reduction based attenuation measurement of earmuffs in a directional sound field

Marc-André Gaudreau[1], Franck Sgard[2], Frédéric Laville[1], Hugues Nélisse[2]

[1]École de Technologie Supérieure, Department of mechanical engineering, 1100 rue Notre-Dame, Ouest, Montréal (Qc), Canada, H3C 1K3
Marc-andre.gaudreau@cegepdrummond.ca

[2]Institut de Recherche Robert-Sauvé en Santé et Sécurité du Travail, 505 Boul. de Maisonneuve, Montréal (QC), Canada, H3A 3C2

Keywords: Hearing protection, continuous F-MIRE, Finite element model; Perfectly matched layer, HPD field attenuation

ABSTRACT

The real attenuation of hearing protection devices (HPD) can be assessed in the field using a method based on continuous field microphone-in-real-ear (F-MIRE) measurements. The two-microphone method provides an indicator called the measured noise reduction (NR^*), defined as the difference between the measured exterior (outside the protector) and interior (under the protector) sound pressure levels (SPL). The HPD's attenuation expressed in terms of the more common insertion loss (IL) can then be obtained from NR^* using compensation factors. For earmuffs, NR^* has been shown to vary of up to 20dB depending on the angle of incidence of the sound source. Therefore, there is a need to use sound incidence dependent compensation factors to relate NR^* and IL. To evaluate these factors and more generally to improve the continuous F-MIRE method, a finite-element (FE) model of an earmuff on an ATF (acoustic test fixture) exposed to a directional sound field has been developed and its predictions compared with lab measurements for several incidence angles. Regarding the external microphone SPL and the NR^*, in one-third of octave bands, the model correlates very well with measurements for frequencies below 1250Hz whatever the sound incidence. Above 1250 Hz, the FE model captures the trends, as a function of the incidence angle, but the agreement generally decreases with increasing frequency. A better correlation between the FE model and the experimental data is achieved for the variation of NR^* (ΔNR^*) as a function of the sound incidence. Actions, such as (i) accounting for the headband in the model, (ii) refining the modeling of the sound source, (iii) improving the cushion modeling and (iv) better describing the backplate/cushion coupling conditions, are suggested to improve the model accuracy. To illustrate the potential of the modeling to improve the continuous F-MIRE measurement method, the FE model is used to determine an optimal

position of the external microphone and to obtain estimates of exposure levels using the left and right ear exterior microphones.

I. INTRODUCTION

Even if noise reduction at source or along the sound propagation path should always be prioritized, individual hearing protection remains the most common way to prevent workers from being exposed to high noise levels. While regularly ineffective, it remains a solution deemed low-cost and easy-to-implement. The present paper focuses on one of the issues associated with the use of hearing protection devices (HPD): the knowledge of the on-site actual individual attenuation that they provide. The standard attenuation ratings for HPDs are obtained under laboratory conditions with subjective or objective methods. The most widely used subjective method is the REAT (real-ear attenuation at threshold) method that aims at evaluating the difference between the perceived sound with and without the HPD. The most widely used objective method is the MIRE (microphone-in-real-ear) method that relies on the measurement of the insertion loss (*IL*), which stands as the difference between the sound pressure at the tympanic membrane with the HPD and without the HPD.

To assess the field attenuation of HPDs, field measurement methods have been developed based on the MIRE method [1–5]. However, in field conditions, measuring the real attenuation a worker gets in a continuous manner is quite impractical as it would require measuring both the protected and the unprotected ears simultaneously, under the exact same sound field. To address this issue, a field counterpart of the MIRE method was developed, the F-MIRE method [6]. F-MIRE uses a microphone doublet to simultaneously measure the sound pressure outside the HPD and inside the ear canal for earplugs or inside the internal air cavity for earmuffs. The difference of the two sound pressure levels gives an approximation of the attenuation of the HPD called “measured noise reduction”, noted NR^*. To estimate the *IL* value, the NR^* has to be corrected by several factors called compensation factors[7,8]. The F-MIRE method was originally developed for earplugs and for “individual fit-testing”[6], i.e. to provide a fast individual measurement of field *IL* by exposing a worker, fitted by an instrumented earplug, to a frontal incidence

sound field generated by a reference loudspeaker. The method used statistical comparisons with REAT measurements to correct the NR^* values and get an approximate IL. Later, the F-MIRE method was extended to earmuffs and was used to provide continuous measurements on workers during their work shifts [9]. However, this study, together with several laboratory experimental studies from the authors of the present papers and others [10–13] found a repeatable frequency dependent relationship, with variations of up to 20dB per third of octave band, of the measured attenuation with the angle of incidence of the sound source. Consequently, as many workers can be exposed to such a directional field when working close to a noise source where the direct field dominates the reverberant background noise, it appears that, when estimating IL from NR^*, using compensation factors that are no longer constant but may vary with sound source incidence should be a necessary improvement of the continuous F-MIRE measurement method.

In order to investigate how this improvement could be achieved, a finite-element model (FEM) of an earmuff exposed to a directional sound field has been developed. Such a model could also help to solve other open questions about the method like the position of the microphones. For earmuffs, the microphone positions are usually chosen in order to minimize the interference with the worker's tasks [14]. However, this does not necessarily correspond to the "optimal" positions.

For the external microphone, the "optimal" position refers to the one that gives the best approximation of the exposure sound field (level without the presence of the head), for all incidence angles. The difference between the exposure sound field and the sound pressure measured by the external microphone is related to the sound scattering by the earmuff, the head and the torso. In the literature some recent experimental work can be found on the effect of the external microphone positioning on the earcup of an earmuff [15], but the work is limited to 6 microphone positions and the results were averaged to get a single value and no modeling work on the position of either microphone could be identified in the literature.

In the past, analytical and numerical models of the occluded ear (earplugs and/or earmuffs) have been developed. The first models, mainly analytical (lumped parameters models), date back from the 50's [16–18] and were improved along the years [19,20]. These models are valid at low frequencies. At mid and high frequencies, geometrical and physical details of the ear and HPD must be accounted for. With computational capacities rapidly increasing, from the mid-90s, numerical models have been found helpful to understand the physical behavior of the protected hearing system in a large frequency range. They all rely on the finite element method (FEM) and/or the boundary element method (BEM) [21–28]. Recent studies have shown the potential of modeling tools such as the FEM to predict and understand the acoustical behavior of HPDs [29–32]. Numerical models dealing with sound transmission through the HPD usually reduce the geometrical complexity of the problem by neglecting the scattering effect induced by the head and torso and rather consider a half space model where the head and torso are replaced by an infinite rigid baffle. Knowing that the sound attenuation of an earmuff is affected by the incidence of the exciting sound field, the infinite baffle simplification cannot be used to address such a problem. In addition, the well-known head-related transfer function (HRTF) can no longer be used to predict the sound pressure at a point close to the earcup as it introduces a significant change in the head and torso geometry.

Consequently, a simplified FEM model was developed that includes the effect of the incident sound field scattering by the head, torso and earcup. To simplify the model development and its validation an ATF (acoustic test fixture) representative of a human head and torso and wearing an earmuff has been used instead of a real human subject. To remove possible errors due to the lack of knowledge regarding the mechanical coupling of the acoustic foam with the pinna and the earcup, the studied configuration does not consider the presence of the pinna and the acoustic foam inside the earcup. The developed numerical model

reproduces this configuration and simulates the F-MIRE measurement (NR^*) of an earmuff coupled to an ATF excited acoustically by plane wave of various incidences.

The theoretical formulations associated with the F-MIRE measurements are presented in section II. The model is detailed in section III and the associated experimental set-up used for the validation is described in section IV. Section V deals with the model validation in three steps: (i) the scattering effect of the ATF protected by an earmuff, (ii) the transmission through the earmuff using NR^* and (iii) the variation of the earmuff measured noise reduction (ΔNR^*) as a function of the sound. Finally, section VI gives an example of application of the model for guiding the selection of the optimal position for the external microphone.

II. THEORETICAL FORMULATIONS OF F-MIRE MEASUREMENTS

In order to present the measurement issues associated with the F-MIRE measurement method, the theoretical expressions associated with this method are illustrated in a synthetic form in Fig. 1. These expressions are adapted from the developments proposed in previously published works of some of the authors of the present article [6–8].

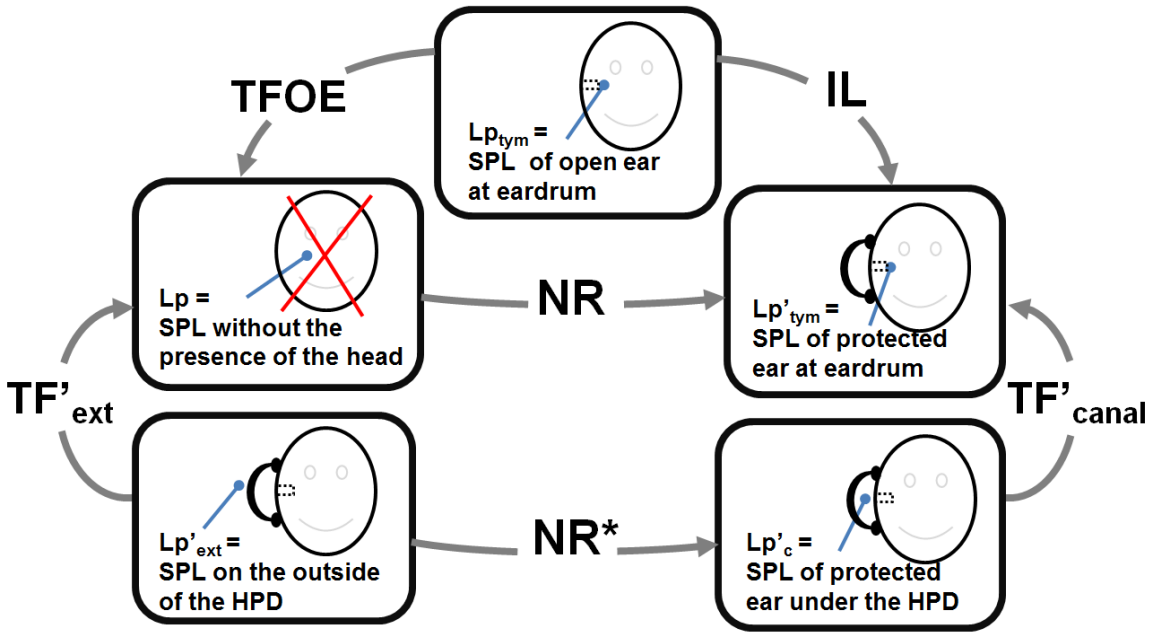

Figure 1 : Diagram of the theoretical expressions associated with the F-MIRE measurement method (indicators in the middle of a gray arrows = value in the box at the arrow origin - value in the box at the arrow head)

The measured noise reduction (NR^*), which is obtained with the F-MIRE method, is given by:

$$NR^*(f) = 20\log_{10}\left(\frac{p'_{ext}}{p'_c}\right) = Lp'_{ext} - Lp'_c \quad (1)$$

where p'_{ext} and Lp'_{ext} are respectively the root mean square sound pressure and the sound pressure level (SPL) at the external microphone. And p'_c and Lp'_c are the root mean square sound pressure and the SPL at the internal microphone. The prime symbol (') denotes the occluded ear conditions.

NR^* is not to be confused with the noise reduction (NR) and the insertion loss (IL), defined by :

$$IL(f) = 20\log_{10}\left(\frac{p_{tym}}{p'_{tym}}\right) = Lp_{tym} - Lp'_{tym} \quad (2)$$

and :

$$NR(f) = 20\log_{10}\left(\frac{p}{p'_{tym}}\right) = Lp - Lp'_{tym} \quad (3)$$

where p (without indices) is referred to as the root mean square sound pressure without the presence of the head of the subject and can also be referred as the exposure sound pressure.

The relation between NR^* and NR can be seen in Figure 1 and is given by :

$$NR = NR^* + TF'_{canal} - TF'_{ext} \quad (4)$$

where TF'_{canal} is the transfer function between the internal microphone root mean square pressure p'_c and the tympanic membrane root mean square pressure p'_{tym} :

$$TF'_{\text{canal}}(f) = 20\log_{10}\left(\frac{p'_c}{p'_{tym}}\right) = Lp'_c - Lp'_{tym} \quad (5)$$

and TF'_{ext} is the transfer function between the external microphone root mean square pressure p'_{ext} and the sound exposure root mean square pressure p :

$$TF'_{\text{ext}}(f) = 20\log_{10}\left(\frac{p'_{ext}}{p}\right) = Lp'_{ext} - Lp \quad (6)$$

IL values can be obtained from *NR* values as long as the latter are compensated by the transfer function of the outer ear (*TFOE*) [33], giving :

$$IL = NR + TFOE \quad (7)$$

Thus, the relation between NR^* and IL can be written as:

$$IL = NR^* + TF'_{canal} - TF'_{ext} + TFOE \quad (8)$$

In a recent paper [8], these relations, or a combination of them, have been evaluated from laboratory measurements on human subjects, with different earmuff and earplug models. Results from this study are a first step towards implementing valid and precise compensation factors for the F-MIRE field measurements. However this study was limited to a diffuse sound field.

Several other studies using a difference between two microphones (inside and outside of the HPD) have been published in the last decade [9,14,34–36]. If some authors have suggested some compensation factor to relate NR^* to IL, none have taken into account the variation due to the incidence of the sound field. While studies have been made on the influence of the sound incidence on the $TFOE$ [37–40], no study dealt with the other compensation factors TF'_{ext}, TF'_{canal} and NR^*. An example of a model that allows the user to give a correction for the angle of incidence of the sound field is the AHAAH model (Auditory Hazard Assessment Algorithm for Humans) developed by the US military for blast exposures [41-43]. However the model's incidence correction is solely contained in the TFOE and does not account for the other correction factors discussed in the current section.

Even if more work is needed on each of the different indicators discussed above, NR^* is the main basic raw attenuation measurement data available in the F-MIRE method. Studying its variation as a function of incidence is viewed as a first step towards an IL evaluation that will take into account the effect of sound incidence. The current study then focuses on this one indicator: NR^*.

III. NUMERICAL MODEL

The configuration of interest, depicted in Figure 2, consists of an earmuff coupled to an ATF through a silicone disk that simulates the skin. The ATF is a G.R.A.S CB-45® (GRAS Sound & Vibration, Denmark) and the earmuff is an EAR1000 model® (3M Hearing Protection, U.S.A.). The system is excited acoustically by an incident plane wave. As the model accounts for the sound transmission through the earmuff/external ear coupled system, several difficulties occur due to the complex nature of the configuration of interest. It was therefore decided to start this modeling effort with a slightly simplified system obtained by removing the pinna from the ATF and by taking out the foam inside the earcup.

a) 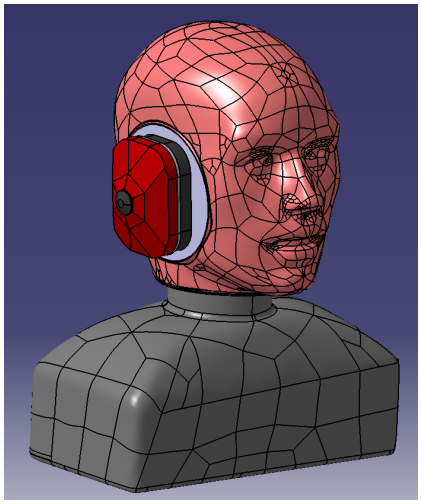 b) 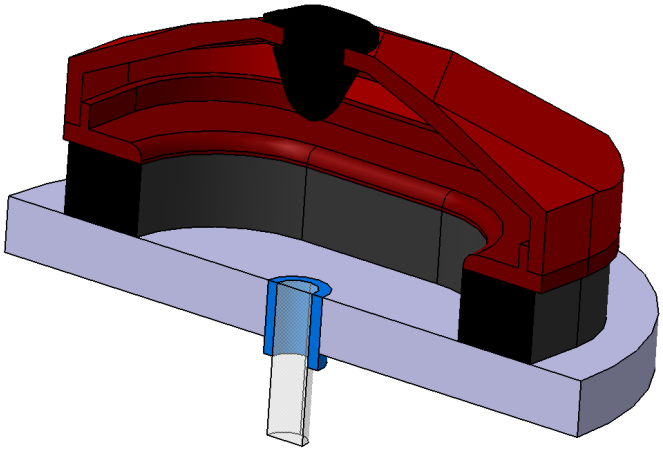

Figure 2 : CAD representation of the different domains, a) Complete view of the CAD, ATF, silicone disk and complete earmuff assembly. b) Cut-away view of the earcup, the comfort cushion, rubber plug, the ear canal skin and the ear canal.

The full geometrical model consists of several domains: (A) the earmuff, (B) the artificial skin insert, (C) the skin inside the ear canal, (D) the earmuff acoustic cavity and the ear canal, (D) the air surrounding the head and torso/earmuff system. The modeling of these domains together with that of the acoustical excitation (E) is discussed in the following subsections. The initial geometries of the earmuff and of the ATF were built using the CAD software Solidworks® (DS, France) and converted to Catia V5® (DS,

France)) for addition of the internal air cavities. The coupled problem is solved using the Finite Element method. All the calculations have been carried out in the commercial software Virtual.Lab 13.2® (LMS/SIEMENS, Germany). The earmuff-earcanal system (see Figure 3) was meshed using Femap V10.2 (Siemens, Germany) whereas the external surrounding air was meshed using Virtual.Lab 13.2 meshing tools (see Figure 3 and Figure 4).

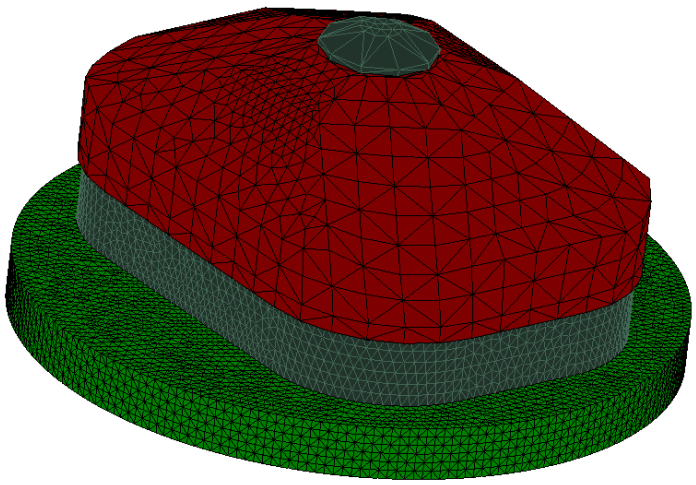

Figure 3 : Meshing of the plastic shell, comfort cushion, rubber plug and artificial skin pad

a) 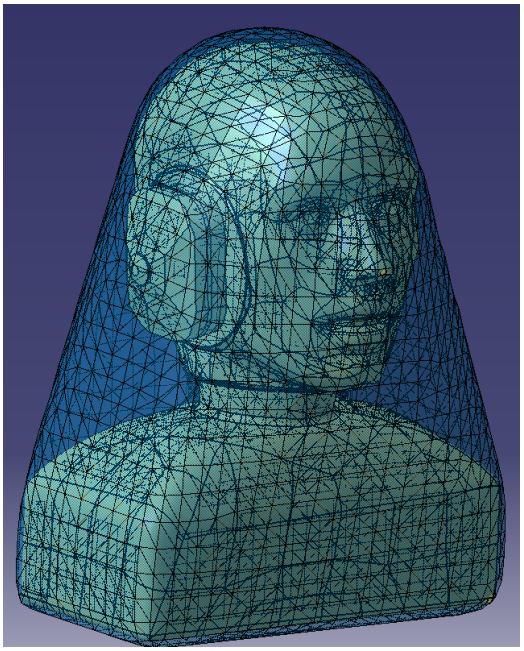 b) 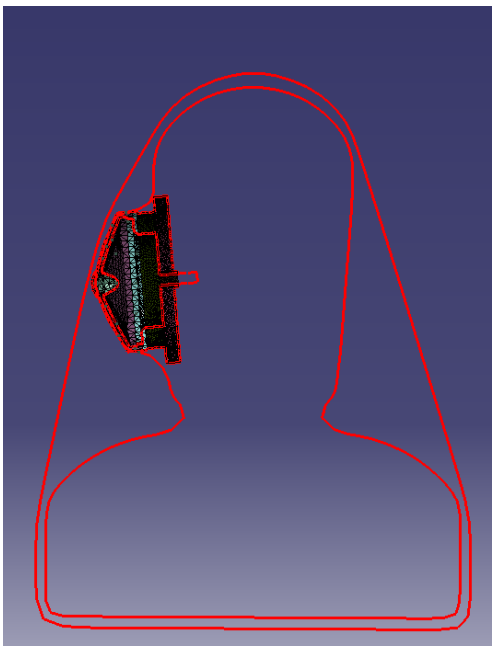

Figure 4 : Meshing of the external surrounding air domain. a) meshing of the surrounding air domain. b) complete cut view of the domains, with the outer line representing the AML and the inner line the ATF boundaries

A. Earmuff modeling

An earmuff is usually composed of 4 main elements: a plastic earcup, a comfort cushion made of an annular polymeric sheath filled with air and foam, a sound absorbing foam pad that is placed inside the plastic envelope, and a headband that, not only links the left and right muffs, but also induces a static force on the earcups to hold them in place against the head and ensure the acoustic seal between them and the head.

For the earmuff of interest, EAR1000 model® (3M Hearing Protection, U.S.A.), there are 5 elements to consider : (i) the plastic earcup, (ii) the comfort cushion, (iii) a rubber plug that links the plastic earcup with (iv) the headband and (v) the sound absorbing foam pad. In this study, only the first 3 elements (i, ii

and iii) are geometrically modeled. The effect of the headband is accounted for in the model by using the compressed cushion static thickness of 12.9mm and its associated mechanical properties [31]. Recall that in this paper, the sound absorbing foam pad has been removed from inside the shell in order to limit the possible sources of error in the model.

In the following, usual displacement and stress vector continuity are applied between solid domains and normal displacement and stress vector continuity between fluid and solid domains. The various domains discretization into finite elements are based on a 4 elements per wavelength meshing criterion.

A-i Plastic earcup

The plastic envelope is assumed linearly elastic and isotropic. It is discretized using 11700 quadratic tetrahedron solid elements. The thermoplastic earcup physical parameters were derived from the literature [44](ρ=1200 kgm^{-3}, E=2.16 GPa, ν=0.38 and η=0.05).

A-ii The Comfort cushion

The earmuff cushion considered here is a complex assembly made up of a thin rubber sheath with vent holes surrounding a comfort foam. It is usually modeled as a spring-damper system [18] or as an equivalent 3D homogeneous isotropic solid. For this model, a different approach was used based on Boyer's research [44], where the cushion is modeled as an equivalent viscoelastic material with a complex Young's modulus. Usual equivalent solid models work well at low frequencies and at high frequencies especially when the acoustical excitation acting on the cushion is neglected but it was found that there is a frequency region (between 1kHz and 2.5kHz for the EAR1000) where the equivalent solid model does not capture correctly

the acoustic transmission phenomena probably because the actual cushion should be modeled as a multilayered system [31,45]. In this work, Boyer's approach to describe the cushion was adopted since to the authors' knowledge it is, up to now, the most complete model. The viscoelastic properties and geometry were taken from the literature[21] (ρ=142.8 kgm^{-3}, ν=0.4 and η=0.36, see [21] for frequency dependent Young's modulus E values). The cushion was discretized using 56000 quadratic tetrahedron solid elements.

A-iii The rubber plug

The rubber plug is considered as a linearly elastic isotropic domain discretized using 430 quadratic tetrahedron solid elements. The rubber physical parameters were derived from the literature [44](ρ=806 kgm^{-3}, E=1 GPa, ν=0.48 and η=0.5).

B. Artificial skin model

The artificial ear and skin insert on the side of the head was replaced by a silicone pad (silicone solutions SS-5060 Shore 00-60) of estimated properties taken from [44] (ρ=900 kgm^{-3}, E=340 kPa, ν=0.48 and η=0.1). The disk of radius 57.5mm and 10mm thickness was discretized using 164000 quadratic tetrahedron solid elements. The silicone boundary in contact with the ATF was assumed to be clamped. Note that the disk's outer surface is coupled to 3 domains: the air cavity inside the earmuff, the cushion and the air surrounding the whole system.

C. Skin inside the ear canal

The normal ear canal of a human is made of 2 sections, the first part (closer to the tympanic membrane) is harder and is called the bony part, while the second part (closer to the outer ear) is softer and is referred to as the elastic cartilaginous part. The ear canal of the ATF is also divided in two sections, the elastic cartilaginous part consists of a steel tube covered with a 2mm thick layer of silicone (length of 13mm), while the second part is made up of steel. This silicone exhibits properties comparable to those of a typical human ear canal, including the skin and the cartilage parameters. Its properties were derived from the literature [46] (ρ=1150 kgm^{-3}, E=420 kPa, ν=0.43 and η=0.2). The silicone layer was discretized into 1560 quadratic tetrahedron solid elements. The steel section of the canal is considered as rigid acoustically.

D. Acoustic cavity and ear canal

The acoustic cavity inside the earmuff is delimited by the plastic shell and the comfort cushion of the earmuff, the artificial skin, the ear canal skin and the tympanic membrane. The mesh consists of 4 000 quadratic tetrahedron acoustic elements. The ear canal is terminated by an ear simulator (IEC 711) which replaces the eardrum and a portion of the ear canal. The ear simulator effect is modeled as a normal acoustic specific impedance boundary condition that is applied to the corresponding area [45].

E. External fluid

FEM operates on finite extent domains. To model the sound propagation in an infinite fluid medium, several numerical techniques have been proposed in the past namely the boundary element method (BEM)[25] , the approach using infinite elements based on a prolate spheroidal multipole expansion [47] and more recently the technique relying on absorbing elements also called the Perfectly Matched Layer

(PML) approach. The PML is coupled to a finite fluid domain enclosing the radiating or scattering object. This domain is discretized with acoustic finite elements. The PML approach is used in this work to account for the coupling of the head/torso/earmuff system with the external fluid domain. PML was originally formulated by Berenger for use with Maxwell's equations [48] and adapted later to the linearized Euler equation known to support acoustic waves [49,50]. The PML consists of a layer or several layers of a fictitious material with an exponential damping factor, working as a perfectly absorbing region for radiated waves, thus avoiding numerical boundary reflections. The thickness of the PML should vary with the wavelength which means that the mesh should be rebuilt at each frequency of interest. In order to decrease the computational time, Virtual.Lab® (LMS/SIEMENS, Germany) developed a new approach where the PML domain is automatically meshed at each frequency at the solver level. In Virtual.Lab, it is called AML for "Automatically Matched Layer".

An automatic function in Virtual.Lab® (LMS/SIEMENS, Germany) generates a convex mesh air domain around the earmuff and ATF (see Figure 4). It was discretized using 23 300 quadratic tetrahedron acoustic elements. The ATF boundary is considered as acoustically rigid. Fluid-structure coupling conditions (continuity of normal displacements and of stress vectors) apply on the cup and skin interface. The convex volume outer surface is coupled to a perfectly matched layer. By doing so, the acoustic waves radiated and scattered by the earmuff in the external domain satisfy the Sommerfeld condition[51].

F. Excitation sound source

The acoustical excitation consists of a unit amplitude plane wave propagating in the horizontal plane going through the head center. The calculations are carried out for several angles of incidence ranging from

0° to 345° degrees with 15 degree steps, 0° being the frontal incidence and 270° pointing directly at the right ear (see Figure 5).

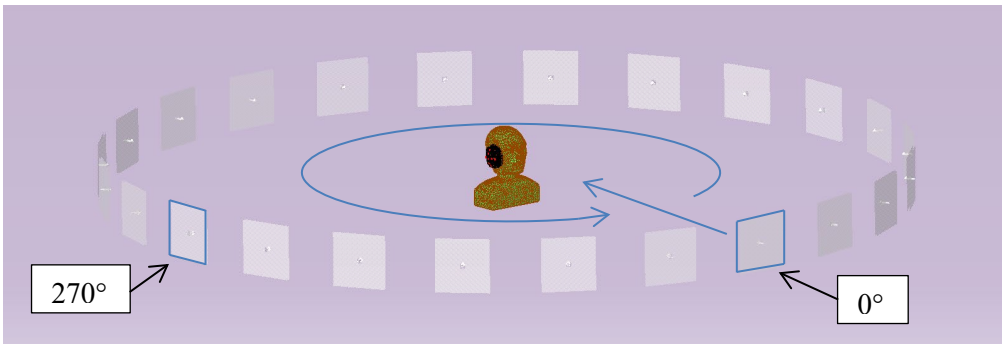

Figure 5 : schematic of the incident plane waves in the horizontal plane around the head for the right ear (with 0° = frontal incidence, 270° = direct incidence)

IV. EXPERIMENTAL SETUP

In order to validate the model, an experimental test setup was designed. The test rig consists of an earmuff (EAR1000) coupled to a standard ATF (G.R.A.S. CB45). As mentioned in the introduction two simplifications were brought to the system: (1) the sound absorbing foam was removed from the earcup to reduce the sources of possible error related to the modeling of this material, (2) the usual silicone pinna and surrounding skin insert of the ATF was replaced by a homemade silicone pad whose properties are well known (see Figure 6). The IEC 711 ear simulator inside the ATF consists of a rigid canal terminated by a microphone whose acoustic impedance corresponds to an average human eardrum and a part of the ear canal. The headband static force applied on the earmuff once positioned on the ATF was measured at 11.5 N, using a dynamometer. The resulting thickness of the compressed cushion was 12.9mm.

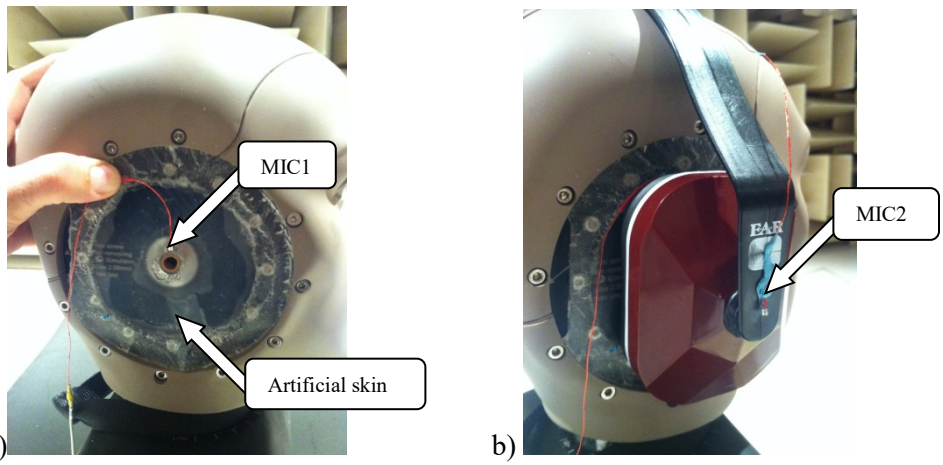

Figure 6 : Experimental test set up showing the Artificial skin (silicone pad) replacing the artificial pinna; (a) without earmuff, showing the internal microphone MIC1; (b) with earmuff, showing the external microphone MIC2

For the experiment, a microphone (MIC1) was placed inside the earmuff, measuring the internal acoustic pressure (p'_c), close to the ear canal entrance (see Figure 6a) and a second microphone (MIC2),

measuring the external acoustic pressure (p'_{ext}), was positioned outside the plastic envelope on the attachment of the headband (see Figure 6b). The relation between p'_c and p'_{ext} is described in equation 1.

The measurements were performed in a semi-anechoic room with a motorized arch hanging from the ceiling (see Figure 7). The extremity of the arch holds a sound source (2-way loudspeaker) directed towards the ATF center and delivering a pink noise of 89dB(A) at 1m. The loudspeaker describes a horizontal circle with a 1 meter radius at the ear height (1 meter above the ground). The ground within that circle was covered with absorbing material to limit the ground reflections.

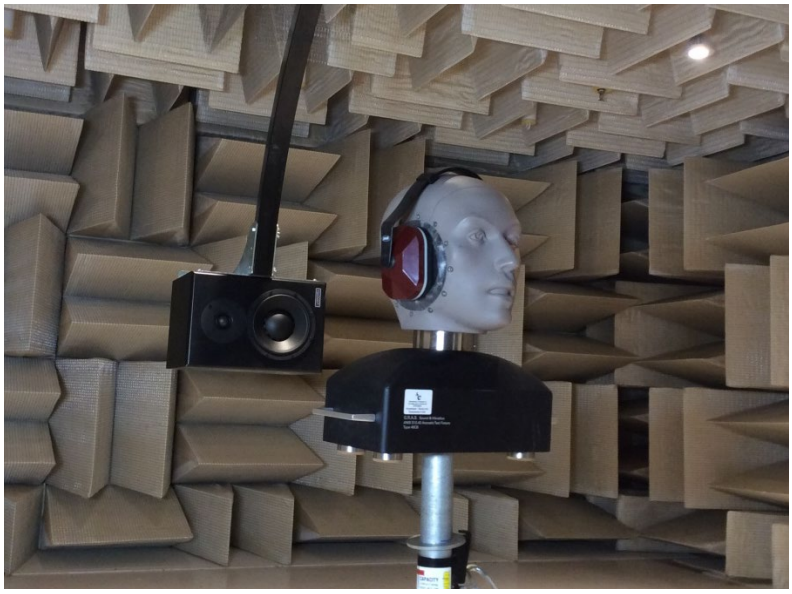

Figure 7 : Experimental set-up, sound source revolving around an ATF with the right ear instrumented and protected with a modified EAR1000 earmuff

V. EVALUATION OF THE FINITE ELEMENT MODEL

This section will present the evaluation of the FE model and is divided in three subsection labeled A, B and C. The first evaluation (subsection A) of the FE model concerns the scattering effect that will show

how the model takes into account the effect of the head/torso/earmuff. These results will also be used in the application presented in section VI, discussing the effect of the external microphone position on the earmuff sound attenuation. The second evaluation (subsection B) deals with the ability of the model to predict the sound attenuation provided by the earmuff. The data will be presented for NR^* as a function of the frequency for different angles of incidence but also as a function of angle of incidence for different frequencies. The third evaluation (subsection C) will address the ability of the model to take into account the variability of the attenuation (ΔNR^*) as a function of the incidence angle.

To validate the coupled AML/FEM approach implemented in the commercial software Virtual.Lab, the acoustical response of a simple system consisting of a rectangular cavity backed simply supported plate embedded in a rigid baffle and excited by an oblique incidence plane wave was first considered. This configuration can be solved semi-analytically [52] using a modal superposition technique for both the plate and the cavity. The comparisons for the sound pressure level inside the cavity between Virtual.Lab and the semi-analytical approach showed an excellent agreement.

The simulation results are now compared with measured data obtained with the experimental set-up presented in the previous section. Both the external sound pressure level (SPL) induced by the scattering of the ATF/earmuff system and the variation of the earmuff's attenuation as a function of the incidence angle of the exciting acoustic plane wave are investigated. All the results are presented in selected one-third octave bands between 50 and 5000Hz, over a complete rotation (360 degrees). For the sake of conciseness, three of the one-third octave bands were chosen as indicators of the whole spectrum. The following figures will therefore show only the 630Hz, 1250Hz and 4000Hz bands, giving a general overview of low, mid and high frequency bands.

A. Comparisons between calculations and measurements: scattering effect (outside microphone)

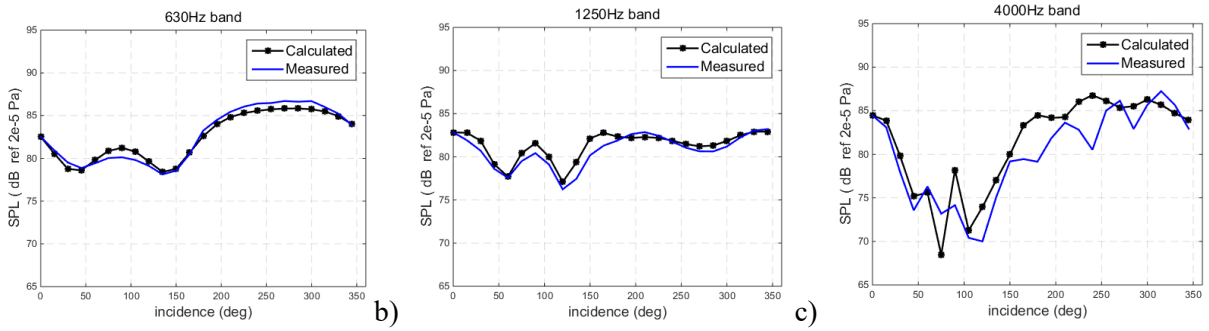

Figure 8 : comparison between predicted and measured third octave band SPLs for the external microphone as a function of the incidence angle for the right ear (as shown in Figure 5)

This subsection presents the comparisons between the experimental data and simulation results for the sound pressure level at the external microphone for the earmuff/ATF configuration. **Erreur ! Source du renvoi introuvable.** shows typical results for the SPL as a function of the incidence angle in three of the one-third octave frequency bands (630, 1250 and 4000Hz). The model is able to capture the trends observed in the measurements. The agreement generally decreases with increasing frequency: it is excellent at low frequencies (< 2dB at 630Hz) and mid frequencies (<3dB at 1250Hz). At high frequencies, the model predicts the trends even if there are larger differences for certain angles of incidence (< 8dB in the 4000Hz band). In this frequency range, the headband that is not included in the model may have an influence on the scattering of the sound field. The discrepancies between the model and the measurement could also be due to the difference between the sound source used in the model (plane wave) and in the experiments (2-way loudspeaker located one meter from the head). Note that a monopole source has also been used in the calculations instead of a plane wave for different incidence angles but only differences of less than 3dB were found.

In addition to the model validation, these numerical and experimental results both show how the influence of the scattering increases as the wavelength gets shorter (increasing frequency). Figure 8 shows that in the 630Hz band, the SPL at the external microphone exhibits variations less than 6dB as a function of the incidence angle whereas in the 4000Hz band these variations can reach values of up to 20dB. Below 100Hz (respectively in the 5000Hz band) (not shown here), these variations are less than 1dB (respectively more than 25dB). At low frequency, the wavelengths are larger than the geometry features giving very low scattering effects.

B. Comparisons between calculations and measurements: NR^* as a function of the frequency and of the incidence angle

This subsection is divided in two parts. Firstly, it presents the comparisons between the experimental data and simulation results for NR^* as a function of the frequency for the earmuff/ATF configuration for 3 different excitation angles (see Figure 9). Secondly, NR^* is plotted as a function of the angle of incidence for three different one-third octave bands (see Figure 11).

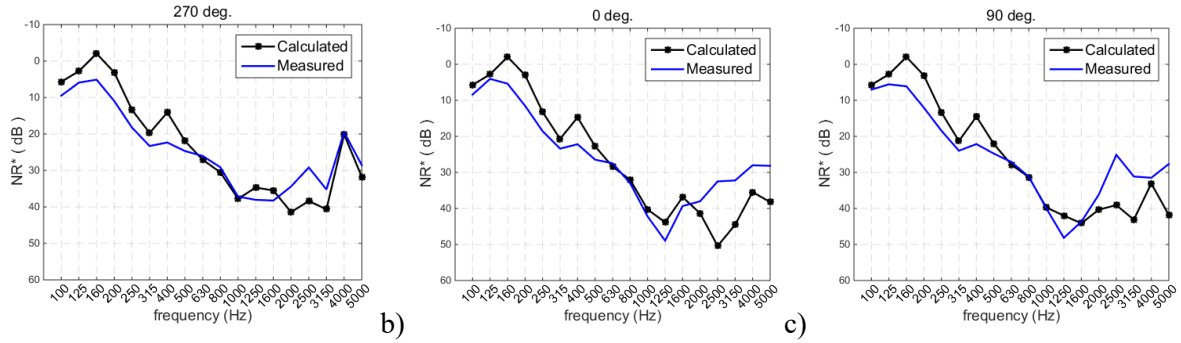

Figure 9 : comparison of predicted and measured one-third octave band $NR^*(f,\theta)$ in (dB) as a function of the frequency for . a) directly exposed side (270°), b) frontal incidence(0°), c) head shadowed side (90°) (see Figure 5 for angle of incidence positions)

Figure 9 shows that, for the different incidence angles, the model is able to capture the overall trends of the noise reduction as a function of frequency. However, the NR^* values are underestimated below 1600Hz and overestimated above 1600Hz.

At low frequency (<1kHz), the experimental curve presents a first peak around 160Hz and a second peak around 400Hz. Both peaks are well captured by the model, but the simulated NR^* values underestimate the lab measurements. In this frequency range, the noise reduction is governed by the pumping motion of the earmuff. The first resonance corresponds to that of the mass of the earmuff coupled to the equivalent spring stiffness of the cushion/ silicone pad/air cavity inside the earmuff system. The second resonance is induced by the presence of the silicone pad (artificial skin) as demonstrated by Figure 10 which shows the results of the calculation where the silicone pad is accounted for and where it is replaced by a rigid material. This effect was also noticed in other measurements made with a steel baffle [44,45]. It can be seen that the effect of the silicone disk is to decrease the pumping frequency because of the equivalent lower stiffness due to the presence of the silicone. Above 1200Hz, the silicone pad has no influence on NR^*. The underestimation of the NR^* could be due to two reasons. First, in the measurement the cushion is not compressed uniformly on the ATF whereas it is in the model. Indeed, in the model, an average compression rate corresponding to a cushion thickness of 12.9mm has been chosen but visual inspection showed important thickness differences between the top and bottom part of the cushion. Yet, as underlined in [31], the equivalent mechanical properties (Young's modulus and loss factor) of the cushion have been shown to be strongly dependent on its compression rate (the more compressed, the higher the equivalent stiffness and loss factor). Second, the mechanical parameters chosen for the silicone used in the artificial skin have been derived from empirical methods based on harshness tests. Therefore, it is likely that these parameters are different from the real ones. A model in which the cushion is divided into several parts with different

compression rates combined with more efficient methods like Dynamic Mechanical Analyzer for the characterization of the silicone pad could probably improve the agreement between model and measurements.

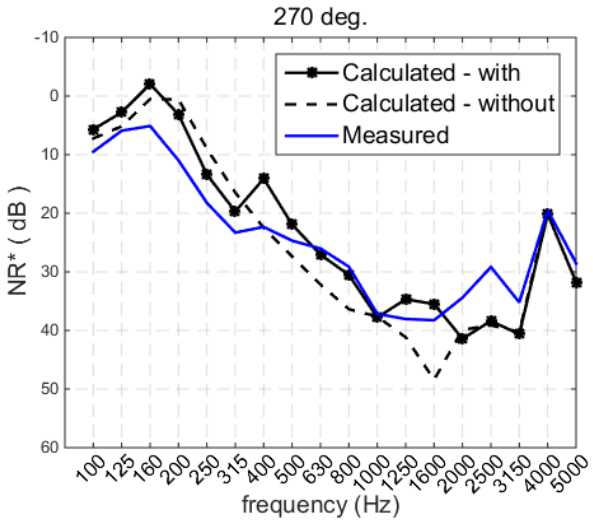

Figure 10 : Effect of the silicone disk, for frontal incidence

In the mid frequency zone (between 1000 and 2500Hz), vibroacoustic coupling effects between the backplate and the comfort cushion are important [44]. The discrepancies observed between the simulations and the measurements are probably due to an inadequate model of the cushion as mentioned previously, together with a poor description of the cushion/backplate coupling conditions (the two components are assumed in perfect contact which may not be true).

At high frequency, the results are influenced by the geometric artifacts on both the measurements and the model. Discrepancies could be explained by the absence of the headband in the model but also by an inadequate model of the real source of excitation.

The following figure gives a different perspective of NR^* values, presenting the data as a function of the angle of incidence for given one-third octave bands.

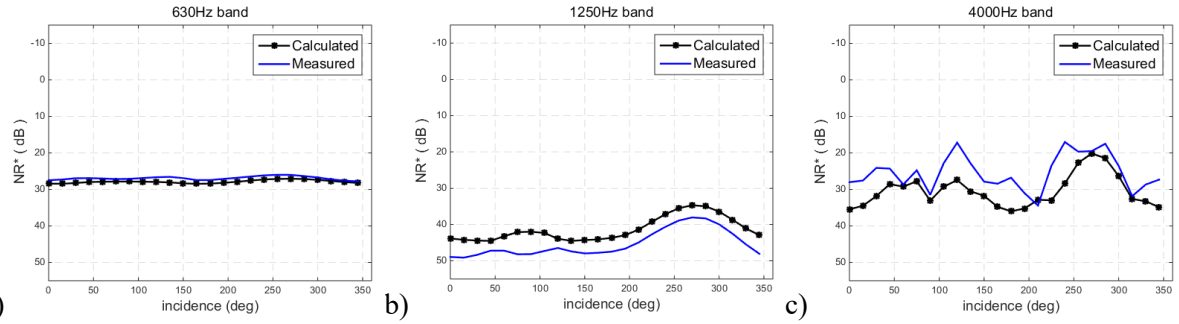

Figure 11 : comparison of predicted and measured one-third octave band NR^* in (dB) as a function of the incidence angle.

Below 1000Hz, the results are generally excellent and as seen on the NR^* spectrum (Figure 9a). Results are similar in other frequency bands except those containing the pumping and silicone pad resonances mentioned previously (160 and 400Hz). More importantly, the model is able to capture the angle of incidence dependence of noise reduction. In the mid frequency zone, discrepancies of up to 8dB between calculated and measured NR^* values occur but overall the model clearly captures well the variation of the NR^* with the incidence angle. As for the high frequency zone, as expected, the amplitudes of NR^* are not well predicted (differences of up to 15dB) but again the trends are captured.

C. Comparisons between calculations and measurements: variation of NR^* (ΔNR^*) as a function of the incidence angle

To better highlight the phenomenon of the variation of the NR^* as a function of the incidence angle, it is useful to normalize the angle-dependant $NR^*(\theta)$ with its value at normal (frontal) incidence $NR^*(\theta=0^\circ)$ to obtain ΔNR^*, that is defined by :

$$\Delta NR^*(f,\theta) = NR^*(f,\theta) - NR^*(f,0^o) \tag{9}$$

Using the variation of NR^* (ΔNR^*) has the advantage, compared to NR^*, to separate the phenomenon related to the variation of the noise reduction as a function of the sound incidence and the absolute noise reduction related to the noise transmission through the earmuff. Since the measured ΔNR^* is the starting point behind the development of this model, its comparison was considered an important step for evaluating the FE model.

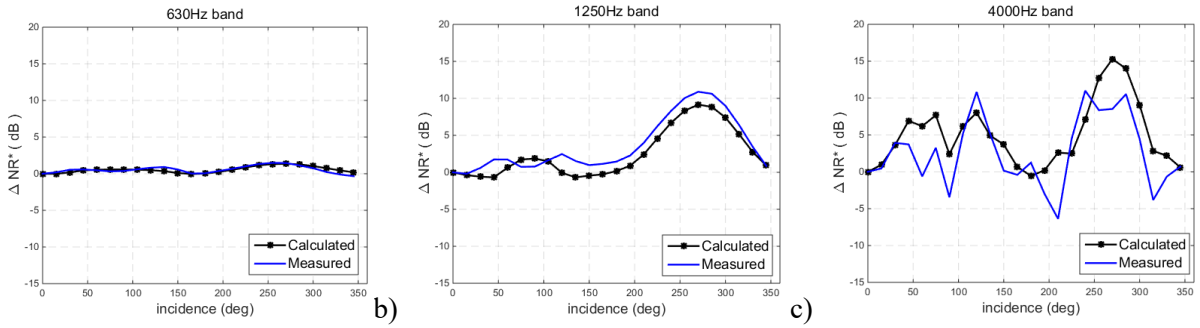

Figure 12 : comparison of predicted and measured one-third octave band ΔNR^* (f,θ) in (dB) as a function of the incidence angle.

Figure 12 compares the measured and predicted ΔNR^* for three one-third octave bands. $\Delta NR^*(f,\theta)$ curves always start with a zero value, since they are normalized with the 0° values. Below 500 Hz (not shown here for the sake of conciseness), experimental and simulated ΔNR^*curves are in good agreement

and are almost flat. A small error (<3db) in the ΔNR^* comparisons is found between the 125 and the 160Hz band due to the experimental measured pumping resonance that fluctuates a few Hz depending on the incidence angle, shifting from one third octave band to the other. At mid frequencies, simulated and experimental ΔNR^*curves are also in very good agreement with maximum differences of less than 3dB up to 1600Hz. Above 1600Hz, the model still captures the trends. Discrepancies between ΔNR^*calculations and measurements are reduced compared to NR^*. Altogether, even if the actual model doesn't succeed in predicting perfectly ΔNR^* at higher frequencies, the model clearly demonstrates its ability to predict the effect of the incidence on ΔNR^*.

VI. APPLICATION OF THE MODEL: FINDING THE OPTIMAL EXTERNAL MICROPHONE POSITION

As stated in the introduction, one of the questions the FE model could help address is finding the optimal position for the F-MIRE microphones. An optimal position for the external microphone can be defined as the one where the measured SPL exhibits the least difference with the exposure level when the sound incidence is varied. In other words, the optimal position is the position that minimizes TF'_{ext}. The external microphone is influenced by the scattering around the ATF/earmuff system. For the internal microphone, the optimal position can be defined as the one that minimizes TF'_{canal}. However, in this paper, the optimal internal microphone position is not investigated. The focus is made on the optimal external microphone position, with the help of the proposed FE model.

One advantage of the continuous F-MIRE method is the ability to obtain readings, in a continuous manner, of the sound field in which a worker is immersed. An optimal position for the external microphone should then also help to find the best estimate of the exposure sound field (the field which

would exist without the presence of the head). In this section, the model is used to find the optimal external microphone position, for one earmuff type (EAR-1000). The SPL is calculated for a set of 40 points randomly distributed covering the outside surface of the earcup (see Figure 13). The exposure sound level is calculated from the simulated power spectral density of the excitation.

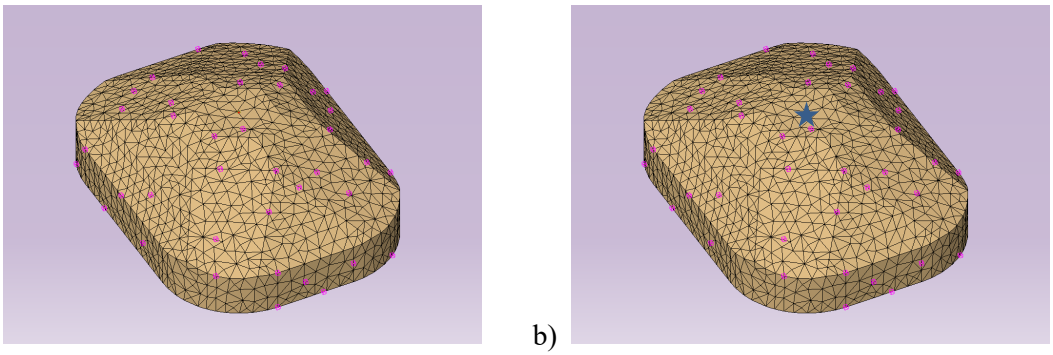

a) b)

Figure 13 : Search for the external microphone optimal position : a) positions of 40 points (randomly distributed) at the surface of the earmuff and b) optimal position located in the center of the surface, represented by a star (blue).

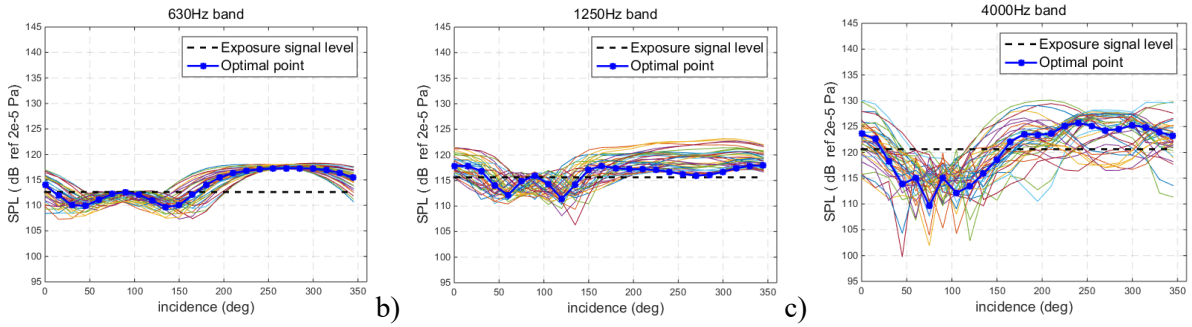

a) b) c)

Figure 14 : Third octave band SPL at the external microphone for 40 points located on the surface of the earmuff (the dotted line shows the exposure signal level).

Figure 14 shows third octave band SPL at the 40 external microphone positions located on the surface of the earmuff for the same three one-third octave bands as those presented in the previous section. When the microphone is in the head shadowed region (0-180 degrees), a lower SPL than the exposure signal level is found as expected. When it is in direct view with the source (180-360 degrees), the SPL will be larger than when it's in the shadow region and can even show more important values (amplification) than the exposure signal level. Such trends are well recovered with the model. The set of curves shown in Figure 14 a) and b) (for 630Hz and 1250Hz bands) give good examples of this, with the 40 different positions following roughly the same pattern. In Figure 14 c) at 4000Hz, the curves become more spread out because of scattering by the studied geometry. In this study, the optimal position for the external microphone is defined as a minimal difference between the exposure root mean square pressure $p(f)$ and the external microphone root mean square pressures ($p_n{}'_{ext}(f,\theta)$, for n = 40). The associated minimization problem can then be written:

$$\min_{n\in[1,40]} \sum_{f_c=50}^{5000} \sum_{\theta=0}^{360} \left| p_n{}'^{2}_{ext}(f,\theta) - p^2(f) \right| \tag{10}$$

where f is the central frequency for one-third octave band between 50 and 5000Hz. θ is the angle of incidence with 15° steps.

Eq(10) yields to the center of the surface of the earmuff as the optimal point (marked by a star in Figure 13 b), this is the same position chosen for the experimental setup. In Figure 14, the solution (thick blue line) exhibits differences of up to 15dBs with the exposure level over a full rotation depending on the angle and the frequency band. This result shows how the outside microphone value, even if optimally positioned, will greatly vary depending on the incidence of the sound source. It also shows that one cannot approximate the exposure level with only one external microphone reading.

As discussed above, the curves are associated with two different spatial regions: the directly exposed side and the head shadowed side. The dividing lines between these two regions are near 0° and 180°, for all the frequency bands. It means that for a given angle of incidence, other than frontal and rear incidence, significant left and right ear differences are expected. Based on this observation, Eq(10) is modified to account for both left ear and right ear external microphones (binaural approach) :

$$\min_{n\in[1,40]} \sum_{f_c=50}^{5000} \sum_{\theta=0}^{360} \left| p'_{binaural}{}^2(f,\theta) - p^2(f) \right| \tag{11}$$

where $p'_{binaural}{}^2$ is obtained by averaging the mean square pressures at both ears (left ear $p'_{ext_{left}}$ and right ear $p'_{ext_{right}}$), namely:

$$p'_{binaural}{}^2(f,\theta) = \frac{p'_{ext_{left}}{}^2(f,\theta) + p'_{ext_{right}}{}^2(f,\theta)}{2} \tag{12}$$

The result of Eq(11) gives the same optimal position as with the previous indicator, the surface center of the earmuff. Figure 15 shows the result for the binaural approach using the optimal external microphone, for 3 third octave frequency bands. Compared with the monaural estimator, the discrepancies between the theoretical exposure level and the estimated exposure level based on microphones located at the surface center of the earcups are now reduced to less than 4dB per frequency band, or less than 2dB for the global pressure level for the studied earmuff. Similar results are obtained in the other frequency bands (not shown here for the sake of conciseness). Since the results are obtained from simulations and that the problem is symmetric (i.e. the microphone is located at the same place for both ears), the results for the left ear were not recalculated but transposed from the right ear results.

The exposure level can therefore be estimated from a measurement of the SPL at the optimal external left ear and right ear microphone whatever the angle of incidence, namely:

$$Lp(f) \approx Lp'_{binaural}(f,\theta) \tag{13}$$

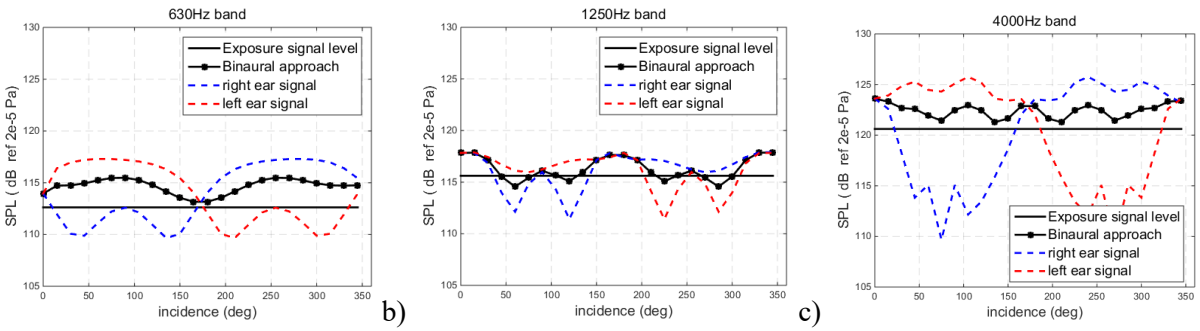

Figure 15 : Comparison between the exposure level and the estimated exposure level. Third octave bands in dB.

Being able to approximate the exposure level is of prime interest for the continuous F-MIRE measurement method as, without modification to the actual method and without knowing the angle of incidence of the sound source, the daily dose of exposition can be approximated. In fact, the error found in the approximation of the exposure level, based on the FE model results, is not larger than the actual dosimetry error caused by the microphone being attached on the shoulder of the worker, as stated in [53] on the effect of the positioning of the dosimeter microphone. Therefore, the binaural approach proposed here seems promising for approximating the exposure level and should be validated in the future with field measurements.

VII. CONCLUSION

In order to evaluate the effect of the sound field incidence on the attenuation of earmuffs measured using continuous F-MIRE, a FE model of a commercial earmuff has been developed. This model takes into account the sound field scattered by the earmuff and the ATF's head-and-torso together with the sound transmission through the earmuff and the ATF artificial skin. The FE model was evaluated by comparisons with laboratory measurements for the SPL at the external microphone and for the earmuff sound attenuation for various sound incidences in a horizontal plane around the ATF. More specifically, three acoustic indicators were considered to compare measurements and calculations: a) SPL at external microphone, b) NR^* and c) ΔNR^*.

For the external microphone SPL comparison, the agreement between tests and simulation is excellent up to 1250Hz (<3dB) and even if larger differences occur at some incidence angles, the model predicts well the trends. To improve the comparisons at higher frequency, the effect of the headband could be studied, either by including it in the model or by modifying the headband in the lab measurements to reduce its effect on scattering. Additionally, the sound source is modeled by a plane wave which is probably not the best approximation of the experimental sound source (2-way loudspeaker at 1m). Using an omnidirectional (monopole) source for the experiments would help reducing the discrepancies at high frequency.

As for the NR^*, the model is able to capture the overall trends with regards to the source position. However, the predicted NR^* values are underestimated below 1600Hz and overestimated above 1600Hz. Below 1000Hz, the two main resonances are captured by the model but NR^* is underestimated compared to the measurements. Accounting for the artificial skin in the FE model improves the correlation between the predicted and measured NR^* notably. Still, a better characterization of the silicone's property and a multi-domain model of the cushion that accounts for variable compression rates would improve the

accuracy of the model. At mid frequency, the discrepancies between simulations and experimental data are attributed to an unsatisfactory cushion model and a bad description of the coupling between the backplate and the cushion. To improve the model at high frequency, the same actions as those discussed before for the external microphone comparisons are suggested

When looking specifically at the variation of NR^* (ΔNR^*), better agreement is obtained compared to NR^* values. The model clearly shows its ability to account for the variation of the noise reduction of the earmuff as a function of the incidence angle of the sound source.

As an example of the utilization of the model to help improving the continuous F-MIRE technique for directional sound field, the model has been used to determine an optimal position of the external microphone. For the earmuff considered in this study, the optimal external microphone position was found to be at the surface center of the earmuff. In addition, a binaural indicator obtained from the average of the mean square pressures evaluated at the external microphone of the right and left ear has been shown to yield a good approximation of the exposure level (mainly less than 2dB, for all frequency bands and incidence angle). This approximation of the exposure level allows for estimating the dose a worker is exposed to, during his work shift. Both the optimal position and the binaural indicator to approximate the exposure level are to be validated with laboratory measurements.

In conclusion, this paper has shown that the acoustic transmission through an earmuff attached to a head and torso in a direct sound field can be captured adequately with the proposed FE model even though the model could be ameliorated. Possibilities for improvement include : 1) accounting for the headband, 2) better modeling the sound source, 3) developing a multi-domain FE model for the cushion, 4) better

describing the backplate/cushion coupling and 5) using mechanical properties obtained from advanced material characterization techniques.

Future works involve (i) evaluating the optimal position of the internal microphone, (ii) accounting for the pinna and the sound absorbing material inside the earmuff, (iii) studying the effect of the incidence angle of the sound source for the complete space around the head (3D), (iv) validating the approximation of the exposure sound field in more complex laboratory and field conditions and (v) studying the variation, as a function of the sound incidence, of the compensation factors (presented in Fig. 1) that relate NR^* to IL.

ACKNOWLEDGMENTS

The authors would like to thank Jérôme Boutin of IRSST for his help during the laboratory measurements and Sylvain Boyer of ÉTS for providing 3D drawings of the GRAS head and torso. They are grateful to IRSST, the FQRNT and to NSERC for providing the financial support of this research project.

[1] Nélisse H, Gaudreau M-A, Boutin J, Voix J, Laville F. Measurement of Hearing Protection Devices Performance in the Workplace during Full-Shift Working Operations. Ann Occup Hyg 2012;56:221–32. doi:10.1093/annhyg/mer087.

[2] Kusy A, Châtillon J. Real-world attenuation of custom-moulded earplugs: Results from industrial in situ F-MIRE measurements. Appl Acoust 2012;73:639–47. doi:10.1016/j.apacoust.2012.02.001.

[3] Kabe I, Kochi T, Tsuruoka H, Tonegawa T, Denda I, Nonogi M, et al. Noise Attenuation of Earplugs as Measured by hREAT and F-MIRE Methods in a Japanese Metal Manufacturing Plant. J Occup Health 2012;54:310–5.

[4] Zera J, Mlynski R. Determination of earmuff transmittance with the use of MIRE technique and with artificial test fixtures. 20th Int. Congr. Acoust. ICA, vol. 2010, 2010.

[5] Kock JFW. Hearing protection in mines: evaluating the Noise Clipper® custom made hearing protection device. Dissertation, Department of Communication Pathology, Faculty of Humanities, University of Pretoria, 2013.

[6] Voix J, Laville F. The objective measurement of individual earplug field performance. J Acoust Soc Am 2009;125:3722.

[7] Gaudreau, Marc-André, Laville F, Nélisse H, Voix J. "Real world HPD attenuation : A new field measurement method using F-MIRE and time signals, NHCA, Atlanta 2009.

[8] Nélisse H, Le Cocq C, Boutin J, Laville F, Voix J. Systematic evaluation of the relationship between physical and psychoacoustical measurements of hearing protectors' attenuation. J Occup Environ Hyg 2015;12:829–44.

[9] Nélisse, H., Gaudreau, M.-A., Boutin, J., Voix, J., Laville, F. Measurement of Hearing Protection Devices Performance in the Workplace during Full-Shift Working Operations. Ann Occup Hyg 2012.

[10] Gaudreau M-A, Laville F, Voix J, Nelisse H. Variabilité de l'atténuation des protecteurs auditifs mesurée par la méthode Field-MIRE en fonction de la direction du son incident et des bruits du porteur. Canadian Acoustic annual conf., Vol. 35, 2007, p. 80–1.

[11] Le Cocq C, Nélisse H, Boutin J, Voix J, Laville F. Influence of source location, subjects and HPD size on the sound field around earmuffs. Canadian Acoustic annual conf., vol. 39 No. 3, Québec: 2011, p. 98–9.

[12] Hagerman B, Olofsson Å, Cheng J, Svensson E. Ear Muff Performance in Impulsive Noise as a Function of Angle of Incidence. Acta Acust United Acust 1996;82:763–71.

[13] Lenzuni P. An educated guess on the workplace variability of ear muff attenuation. Int J Saf Ergon 2009;15:201–10.

[14] Gaudreau M-A, Laville F, Nélisse H, Voix J. Méthode de mesures terrain de l'atténuation F-MIRE de protecteurs auditifs durant un quart de travail. Can Acoust 2008;36:3–10.

[15] Le Cocq C, Nélisse H, Boutin J, Voix J, Laville F. Estimation of noise exposure level for subjects wearing hearing protector devices. Proc. Meet. Acoust. ICA, Montreal, QC, Canada: 2013.

[16] Zwislocki J. An investigation of certain means of sound attenuation at the ear. Syracuse University Research Institute; 1961.

[17] Zwislocki J. Design and Testing of Earmuffs. J Acoust Soc Am 1955;27:1154–63. doi:10.1121/1.1908149.

[18] Shaw EAG, Thiessen GJ. Improved Cushion for Ear Defender. J Acoust Soc Am 1958;30:24–36.

[19] Schroeter J, Posselt C. The use of acoustical test fixtures for the measurement of hearing protector attenuation. Part II: Modeling the external ear, simulating bone conduction, and comparing test fixture and real-ear data. J Acoust Soc Am 1986;Vol. 80:505–27.

[20] Sides JD. Low Frequency Modeling and Experimental Validation of Passive Noise Attenuation in Ear Defenders. Master thesis, Virginia Tech, Blacksburg, Virginia, 2004.

[21] Boyer S, Doutres O, Sgard F, Laville F, Boutin J. Objective assessment of the sound paths through earmuff components. Appl Acoust 2014;83:76–85. doi:10.1016/j.apacoust.2014.03.017.

[22] Chang-Myung Lee, Larry H. Royster, Robert D. ciskowski. Formulation for an FE and BE coupled problem and its application to the earmuffnext term-earcanal system. Eng Anal Bound Elem 1995;16:305–15.

[23] Ciskowski RD, Royster LH. Boundary element solution to predict transient response of a 3-D coupled fluid cavity-elastic structure system. Bound. Elem. Methods Appl. Mech. Pergamon Press, New York: M. Tanaka & T. A. Cruse; 1988, p. 545–54.

[24] Gerges SN, Vergara F, Birch RS. Finite element method (FEM) model for the hearing protector noise attenuation for impulsive noise, Inter-Noise conf.. Nice, France: 2000, p. 4.

[25] Royster LH, Mourad K, Xie KJ, Ciskowski R. Developments in using the boundary element method (BEM) to investigate the dynamic characteristics for foam earplug-earcanal and earmuff-earcanal systems. J Acoust Soc Am 1990;88:S9. doi:10.1121/1.2029247.

[26] Sgard F, Brummund M, Viallet G, Boyer S, Petit Y, Laville F, et al. Acoustic finite element modeling of hearing protection devices. Proc. Internoise 2012, New-York, NY: 2012.

[27] Sgard F, Nelisse H, Boutin J, Laville F, Voix J, Gaudreau M-A. Finite element modeling for the evaluation of sound attenuation of hearing protectors, Euronoise, Edinburgh, UK, 2009.

[28] Xie K-J, Ciskowski, RD, Royster LH. An investigation of wave propagation in viscoelastic media modeled by fractional derivative using the boundary element method. Bound. Elem. Methods Appl. Mech. Pergamon Press, New York: M. Tanaka & T. A. Cruse; 1988, p. 523–31.

[29] Brummund M, Sgard F, Petit, Yvan, Laville F. A simplified axi-symmetric finite element model of the human outer ear to determine the earplug induced auditory occlusion effect. J. Acoust. Soc. Am., vol. 130, No. 4, San Diego, CA, USA: 2011, p. 2469.

[30] Brummund MK, Sgard F, Petit Y, Laville F. Three-dimensional finite element modeling of the human external ear: simulation study of the bone conduction occlusion effect. J Acoust Soc Am 2014;135:1433–44.

[31] Boyer SW, Doutres O, Sgard F, Laville F, Boutin J. Sound transfer path analysis to model the vibroacoustic behavior of a commercial earmuff. J Acoust Soc Am 2013;133:3236–3236.

[32] Viallet G, Sgard F, Laville F, Boutin J. Axisymmetric versus three-dimensional finite element models for predicting the attenuation of earplugs in rigid walled ear canals. J Acoust Soc Am 2013;134:4470–80.

[33] Berger EH. Review and tutorial - methods of measuring the attenuation of hearing protection devices. J Acoust Soc Am 1986;vol. 79:1655–87.

[34] Kotarbinska E, Kozlowski E. Measurement of Effective Noise Exposure of Workers Wearing Ear-Muffs. Int J Occup Saf Ergon 2009;15:193–200.

[35] Kusy A. Affaiblissement acoustique in situ des protecteurs individuels contre le bruit - Étude bibliographique. Cah Notes Doc INRS 2008;212:43–59.

[36] Kusy A, Châtillon J. Real-world attenuation of custom-moulded earplugs: Results from industrial in situ F-MIRE measurements. Appl Acoust 2012;73:639–47. doi:http://dx.doi.org/10.1016/j.apacoust.2012.02.001.

[37] Hammershoi D, Moller H. Sound transmission to and within the human ear canal. J Acoust Soc Am 1996;100:408—427. doi:10.1121/1.415856.

[38] Cheng CI, Wakefield GH. Introduction to head-related transfer functions (HRTFs): Representations of HRTFs in time, frequency, and space. J-AUDIO Eng Soc 2001;49:231–49.

[39] Møller H, Hammershøi D, Jensen CB, Sørensen MF. Transfer Characteristics of Headphones Measured on Human Ears. J Audio Eng Soc 1995;43:203–17.

[40] Takane S, Arai D, Miyajima T, Watanabe K, Suzuki Y, Sone T. A database of Head-Related Transfer Functions in whole directions on upper hemisphere. Acoust Sci Technol 2002;23:160–2. doi:10.1250/ast.23.160.

[41] Fedele P, Binseel M, Kalb J, Price GR. Using the auditory hazard assessment algorithm for humans (AHAAH) with hearing protection software, release MIL-STD-1474E. Aberdeen Proving Ground (MD); Army Research Laboratory (US): 2013 Dec. Report No.: ARL-TR-6748.

[42] Fedele P, Kalb J. Level-Dependent Nonlinear Hearing Protector Model in the Auditory Hazard Assessment Algorithm for Humans. Aberdeen Proving Ground (MD); Army Research Laboratory (US): 2015 April. Report No.: ARL-TR-7271

[43] Kalb J. A hearing protector model for predicting impulsive noise hazard, Proceedings of Noise-Con 2010, Baltimore, Maryland: 2010

[44] Boyer S. Étude de la transmission sonore à travers un protecteur de type "coquilles" : modélisation numérique et validation expérimentale. Thèse de doctorat (Ph.D.). École de technologie supérieure, 2015.

[45] Sgard F, Nélisse H, Gaudreau M-A, Boutin J, Voix J, Laville F. Étude de la transmission sonore à travers les protecteurs auditifs et application d'une méthode pour évaluer leur efficacité effective en milieu de travail - Partie 2 : Étude préliminaire d'une modélisation des protecteurs auditifs par éléments finis. IRSST - Rapport R-680; 2010.

[46] Viallet G, Sgard F, Laville F, Boutin J. A finite element model to predict the sound attenuation of earplugs in an acoustical test fixture. J Acoust Soc Am 2014;136:1269–80. doi:http://dx.doi.org/10.1121/1.4890645.

[47] Burnett DS. A three-dimensional acoustic infinite element based on a prolate spheroidal multipole expansion. J Acoust Soc Am 1994;96:2798–816. doi:10.1121/1.411286.

[48] Berenger, J.-P. A perfectly matched layer for the absorption of electromagnetic waves. J Comput Phys 1994:Pages 185–200.

[49] CHEW, W.C., LIU, Q.H. PERFECTLY MATCHED LAYERS FOR ELASTODYNAMICS: A NEW ABSORBING BOUNDARY CONDITION. J Comput Acoust 1996:Pages 341–60.
[50] Hu FQ. On Absorbing Boundary Conditions for Linearized Euler Equations by a Perfectly Matched Layer. J Comput Phys 1996;129:201–19. doi:10.1006/jcph.1996.0244.
[51] Schot SH. Eighty years of Sommerfeld's radiation condition. Hist Math 1992;19:385–401. doi:10.1016/0315-0860(92)90004-U.
[52] Sgard F, Atalla N, Nicolas J. Coupled FEM-BEM approach for mean flow effects on vibro-acoustic behavior of planar structures. AIAA J 1994;32:2351–8. doi:10.2514/3.12299.
[53] Byrne DC, Reeves ER. Analysis of Nonstandard Noise Dosimeter Microphone Positions. J Occup Environ Hyg 2008;5:197–209.